Journal of the Brazilian Society of Mechanical Sciences and Engineering (2026) 48:246
https://doi.org/10.1007/s40430-026-06348-z

TECHNICAL PAPER

Torsional vibration analysis of viscoelastic functionally graded nanotubes with viscoelastic boundaries using lam's strain gradient theory

Hayrullah Gün Kadioğlu[1] · **Busra Uzun**[2] · **Mustafa Ozgur Yayli**[2]

Received: 12 September 2025 / Accepted: 16 January 2026
© The Author(s) 2026

Abstract
In this study, the torsional vibration of viscoelastic FG nanotubes with viscoelastic boundary conditions has been investigated by considering the size effect. The size effect has been based on the strain gradient elasticity theory developed by Lam. The Kelvin-Voigt viscoelastic model has been employed to model the time-dependent material behavior. In order to solve the problem, an approach has been developed by combining the Fourier Sine series and the Stokes transform. At the end of this process, an eigenvalue problem has been achieved that determines the torsional vibration frequencies of the viscoelastic nanotube under Kelvin-Voigt viscoelastic boundary conditions. The eigenvalue problem provides a general solution including the length scale parameters of the material, the viscous damping coefficient and the viscoelastic boundary conditions. Thus, a highly flexible and efficient solution methodology has been proposed for examining the torsional vibration behavior of viscoelastic nanotubes under viscoelastic boundary conditions. Therefore, the present study is anticipated to provide a substantial contribution to the existing body of literature. The findings obtained from the study are presented in figures and tables; it has been observed that scale parameters and power-law exponent increase the damping effect, and in cases where viscous properties become dominant, the frequencies of higher modes can reach lower values than the first mode.

Keywords Functionally graded materials · Viscoelastic materials · Torsional vibration · Stokes' transformation · Viscoelastic boundary conditions

1 Introduction

Nowadays, nanotechnology has opened a new era by forming a wide range of application areas in various fields. Nanoscience and nanotechnology, which are based on the production, reconstruction and investigation of the properties of nanoscale materials, are quite remarkable. Because the materials discovered and produced with the possibilities of nanotechnology have very different properties than expected and usual. It has been noticed that even small changes in the arrangement, length and bonding patterns of the atoms and molecules that make up such materials can cause significant changes in the properties of the materials. The reason for this change is the size effect detected at small scales. The dimensions must be small enough to notice the size effect. Such changes made at macro dimensions do not cause changes in the properties.

In order to evaluate the properties of small-scale nano/micro materials and structural elements, it is necessary to resort to experimental studies and molecular dynamics simulations. However, they have some disadvantages due to their high costs and long-term requirements. To overcome these and investigate the size effect, higher order elasticity theories [1–6] have been developed. These theories do not require high costs and long time, such as experimental studies and molecular dynamics simulations, and allow the

Technical Editor: Aurelio Araujo.

✉ Hayrullah Gün Kadioğlu
hayrullahgunkadioglu@arel.edu.tr

[1] Technical Sciences Vocational School, Department of Construction, İstanbul Arel University, İstanbul, Turkey

[2] Faculty of Engineering, Department of Civil Engineering, Bursa Uludag University, Bursa, Turkey

Published online: 11 March 2026

size effect to be demonstrated theoretically. These theories, which overcome the size effect with the material length scale parameters they contain, differ from classical theories. Classical theories are not suitable for analysis of nano/microstructures as they do not include any material length scale parameters. On the other hand, some of the higher order elasticity theories have one scale parameter, while some have two or more scale parameters. Some studies conducted in this context are summarized below.

Eltaher et al. [7] investigated the free vibration of perforated viscoelastic nanobeams with non-local theory. Yaylı [8] performed the free vibration analysis of functionally graded (FG) nanobeams using Nonlocal theory for a beam modeled with rotation-restricting springs. Trabelssi [9] investigated the free and forced vibration behavior of nonlocal Timoshenko-type graded nanobeams on a nonlinear elastic foundation using analytical and numerical methods, considering geometric nonlinearities along with Eringen's nonlocal elasticity model. Uzun and Yaylı [10] analytically investigated the free vibration frequencies of nonlocal Rayleigh nanobeams made of functional graded material with four different porosity distributions on a Winkler foundation, considering different boundary conditions, including rotational inertia and flexible spring effects. Kadioglu and Yaylı [11] investigated the free vibration behavior of a viscoelastic FG nanobeam. Balcı [12] analytically investigated the axial forced vibration behavior of viscoelastic, radially graded porous nanorods based on Eringen's nonlocal elasticity theory and the Kelvin–Voigt model. Ahmadi et al. [13] developed a new displacement-based formulation for the free vibration analysis of magneto-electro-elastic (MEE) nanobeams on an elastic foundation, incorporating nonlocal elasticity theory and capable of capturing thickness and bending vibration modes. Mohammed and Hussein [14] investigated the damped torsional vibrations of single-walled carbon nanotubes (SWCNTs) under thermal stresses in a nonlinear viscoelastic medium, considering the nonlinear damping effect of the medium within the framework of the nonlocal Eringen elasticity theory. Zhen et al. [15] investigated the free vibration of viscoelastic nanotubes under longitudinal magnetic field in combination with Timoshenko beam theory and non-local strain gradient theory for cantilever beams. Challamel et al. [16] investigated the free vibration behavior of micromorphic beams using the nonlocal strain gradient theory.

El-Borgi et al. [17]carried out nonlinear vibration analysis of nano-beams by including non-local and surface effects. Mohammadimehr et al. [18] investigated the vibration of tapered micro-rod with viscoelastic material based on the strain gradient theory. Also, the micro-rod rests on Visco Pasternak foundation and the authors used the differential quadrature method for the analyses. El-Borgi et al. [19] studied the torsional vibration of visco-elastic rods based on the size dependency in the context of nonlocal strain and velocity gradient theory. Ansari et al. [20] indicated the torsional vibration frequencies of carbon nanotubes via strain gradient theory. Also, the authors presented the results of classical theory, modified couple stress theory (MCST) and molecular dynamic simulations. Kadioglu et al. [21] investigated the torsional vibration of porous viscoelastic nanorods under viscoelastic boundary conditions.

Civalek et al. [22] performed nonlinear stability analysis of perforated nano-beams utilizing Fourier series. Akgöz and Civalek [23] performed the analysis of micro-sized beams with the modified strain gradient elasticity and modified couple stress theories under rigid boundary conditions. Uzun et al. [24] analyzed the axial and torsional vibration of saturated nanorods using high-order Fourier series obtained with the help of Stokes' transforms. Uzun et al. [25] investigated the torsional vibration of FG porous nanotubes resting on elastic ground using non local elasticity theory under elastic boundary conditions. Uzun et al. [26] proposed a semi-analytical solution for embedded and elastically restrained single-walled boron nitride nanotubes for axial and torsional vibrations based on nonlocal strain gradient theory. Uzun et al. [27] presented the torsional vibration of porous FG strain gradient nanotubes at general (rigid and deformable) boundary conditions. As can be understood, torsional vibration analysis of nano/micro sized rod elements is a subject that researchers focus on, and there are other studies [28–38] on this subject in the literature.

Since the subject of this article is a torsion tube, articles that study torsional vibration based on the size effect of nano/micro rod type elements have been mentioned above. In addition, theories including the size effect are frequently used for various materials and elements. Marinca et al. [39], Chu et al. [40], Boyina at al. [41], Ebrahimi and Barati [42] studied the nonlocal strain gradient theory for FG nanobeams. Boyina at al. [41] realized thermal buckling response, while Marinca et al. [39] and Chu et al. [40] considered nonlinear dynamics of FG nanobeams. Karamanlı [43], Civalek et al. [44], Gül and Aydoğdu [45], Kadioğlu and Yayli [46], Ozmen and Esen [47] handled the doublet mechanics effects on the nanobeams with different solution methods. Ye et al. [48], Atcı [49], Li and Xiao [50] presented the different mechanical responses of microbeams via modified couple stress theory (MCST). In addition to one-dimensional nano/micro-sized elements, analyzes of two-dimensional nano/micro-sized structures based on higher order elasticity theories [51–55] are also very interesting.

In addition to all these, Qiao and Rahmatalla [56] investigated the dynamic behavior of Euler Bernoulli beams under a moving load under viscoelastic boundary conditions. This study is based on the viscoelastic model used by Qiao and

Rahmatalla [56] for viscoelastic boundary conditions. The model used is called Kelvin Voight model in the literature. According to this model, a viscous damper with viscous properties and a spring with elastic properties are connected in parallel. This model has been used by researchers to investigate the viscoelastic properties of the material rather than boundary conditions [57–62]. In addition, in this study, this model is included in the problem not only for boundary conditions but also for material properties.

Finally, this study has achieved the torsional vibration of viscoelastic FG nanotubes with viscoelastic boundary conditions based on the size effect. The Lam's strain gradient elasticity theory has been taken into account to investigate the small-size effect. The main reason for preferring Lam's strain gradient theory is that classical elasticity theories cannot adequately represent size effects in micro- and nanoscale structures, and that high-order deformation effects must be taken into account in order to model these structures in a manner consistent with experimental observations. Both ends of the nanotube have been restrained with torsional springs that permit rotation and a viscous damper. The model has been solved using a combination of Stokes' transform and the Fourier Sine series. Ultimately, a 2×2 eigenvalue problem able to determine the viscoelastic nanotube's torsional vibration frequencies have been derived. Thus, a highly flexible and advantageous solution method has been presented for analyzing the torsional vibration of a viscoelastic nanotube under viscoelastic boundary conditions. In this respect, the study is expected to make a significant contribution to literature. The stiffnesses of torsional springs, material length scale parameters, and viscosity damper characteristics are included in this eigenvalue problem. By assigning these parameters to specific values, results belonging to the classical theory, modified couple stress theory (MCST), only viscoelastic boundary condition, only deformable boundary condition and rigid boundary condition can be obtained.

2 Definition of problem

The strain gradient theory proposed by Lam et al. [4] is used to probe the size effect of nanoscale structures. The governing equations of this theory contain three additional material length scale parameters and the strain energy according to this theory is expressed as follows [4]:

$$U = \frac{1}{2}\int_V \left(\sigma_{ij}?_{ij} + \mathrm{P}_i\gamma_i + \mathrm{T}^*_{ijk}\varkappa^*_{ijk} + \Pi_{ij}\Gamma_{ij}\right) dV \tag{1}$$

Where, the expressions from the classical strain energy $?_{ij}$ and σ_{ij} represent strain expressions and classical stress, respectively. Π_{ij} and Γ_{ij} which are also observed in MCST are the deflecting part of the double stress tensor and rotational strain tensor, respectively. $\varkappa^*_{ijk}$ is the deviatoric strain change tensor and γ_i is the dilatation change vector, as T^*_{ijk} and P_i are higher order stress tensors. When the Kelvin Voigt viscoelastic model is included, all parameters in the strain energy are as follows:

$$\sigma_{ij} = 2\left(1 + t_d\frac{\partial}{\partial t}\right)G(r)\epsilon_{ij} + \alpha\epsilon_{kk}\delta_{ij} \tag{2}$$

$$?_{ij} = \frac{1}{2}\left(\frac{\partial\psi_i}{\partial x'_j} + \frac{\partial\psi_j}{\partial x'_i}\right) \tag{3}$$

$$\mathrm{P}_i = 2\left(1 + t_d\frac{\partial}{\partial t}\right)G(r)\zeta^2\gamma_i \tag{4}$$

$$\gamma_i = \acute{\epsilon}_{mm,i} \tag{5}$$

$$\mathrm{T}^*_{ijk} = 2\left(1 + t_d\frac{\partial}{\partial t}\right)G(r)\gamma^2\varkappa^*_{ijk} \tag{6}$$

$$^*_{ijk} = \frac{1}{3}\begin{pmatrix}\acute{\epsilon}_{ij,k} + \acute{\epsilon}_{jk,i}\\ +\acute{\epsilon}_{ki,j}\end{pmatrix} - \frac{1}{15}\left[\begin{pmatrix}2\acute{\epsilon}_{mk,m}\\ +\acute{\epsilon}_{mm,k}\end{pmatrix}\delta_{ij} + \begin{pmatrix}2\acute{\epsilon}_{mi,m}\\ +\acute{\epsilon}_{mm,i}\end{pmatrix}\delta_{jk} + \begin{pmatrix}2\acute{\epsilon}_{mj,m}\\ +\acute{\epsilon}_{mm,j}\end{pmatrix}\delta_{ki}\right] \tag{7}$$

δ_{ij} (1 for i=j, 0 for i≠j) is the Kronecker delta function. ψ_i and ψ_j are the displacement vector, t_d is the viscous damping coefficient ζ and γ is the material length scale parameter. G(r) is the shear modulus and depends on the modulus of elasticity, denoted by E(r) and Poisson's ratio, denoted by υ, as follows.

$$G(r) = \frac{\mathrm{E(r)}}{2(1+\upsilon)} \tag{8}$$

m_{ij} and Γ_{ij} are as follows.

$$M_{ij} = 2\iota^2\left(1 + t_d\frac{\partial}{\partial t}\right)G(r)\chi_{ij} \tag{9}$$

$$\Gamma_{ij} = \frac{1}{2}(\Phi_{i,j} + \Phi_{j,i}) \tag{10}$$

Φ is the rotation vector, where ι is the third scale parameter indicating the size effect of the material. Φ is proposed by [4]:

$$\Phi_i = \frac{1}{2}\left(\psi_{k,j}e_{ijk}\right) \tag{11}$$

Here, e_{ijk} is the permutation symbol and can take three different values as follows:

$$e_{ijk} = \begin{cases} +1 \, for \quad (i,j,k) = (x,y,z), (y,z,x), (z,x,y) \\ 0 \, for \quad i = j \, or \, j = k \, or \, i = k \\ -1 \, for \quad (i,j,k) = (x,z,y), (z,y,x), (y,x,z) \end{cases} \tag{12}$$

The displacement functions of a nanotube in a three-dimensional plane x, y, z are as follows.

$$\psi_z(x,t) = y\theta(x,t) \tag{13}$$

$$\psi_y(x,t) = -z\theta(x,t) \tag{14}$$

$$\psi_x(x,t) = 0 \tag{15}$$

$\psi_x(x,t)$, $\psi_y(x,t)$ and $\psi_z(x,t)$ are the displacements in the x, y and z directions, respectively, where t is the time. $\theta(x,t)$ refers to the time-dependent torsion angle (angular displacement) of the viscoelastic nanotube. The deformations are obtained by via above displacement functions as follows:

$$\acute{\epsilon}_{xx} = \acute{\epsilon}_{yy} = \acute{\epsilon}_{zz} = \acute{\epsilon}_{yz} = \acute{\epsilon}_{zy} = 0 \tag{16}$$

$$\acute{\epsilon}_{xy} = \acute{\epsilon}_{yx} = \frac{z}{2}\partial_x\theta(x,t) \tag{17}$$

$$\acute{\epsilon}_{xz} = \acute{\epsilon}_{zx} = -\frac{y}{2}\partial_x\theta(x,t) \tag{18}$$

The components of Φ are determined as [20]:

$$\Phi_z = \frac{z}{2}\frac{\partial\theta(x,t)}{\partial x} \tag{19}$$

$$\Phi_y = -\frac{y}{2}\frac{\partial\theta(x,t)}{\partial x} \tag{20}$$

$$\Phi_x = \theta(x,t) \tag{21}$$

The stress tensors of the nanotube are calculated as follows with the help of Eq. (2) and Eqs. (16-18).

$$\sigma_{xz} = \sigma_{zx} = (1 + t_d\frac{\partial}{\partial t})G(r)\, y\frac{\partial\theta(x,t)}{\partial x} \tag{22}$$

$$\sigma_{xy} = \sigma_{yx} = -(1 + t_d\frac{\partial}{\partial t})G(r)\, z\frac{\partial\theta(x,t)}{\partial x} \tag{23}$$

The non-zero components of Γ_{ij} are determined by [20]:

$$\Gamma_{zz} = \Gamma_{yy} = -\frac{1}{2}\frac{\partial\theta(x,t)}{\partial x} \tag{24}$$

$$\Gamma_{xx} = \frac{\partial\theta(x,t)}{\partial x} \tag{25}$$

$$\Gamma_{yx} = \Gamma_{xy} = -\frac{y}{4}\frac{\partial^2\theta(x,t)}{\partial x^2} \tag{26}$$

$$\Gamma_{zx} = \Gamma_{xz} = -\frac{z}{4}\frac{\partial^2\theta(x,t)}{\partial x^2} \tag{27}$$

With the via of Eqs. (24)-(27) and Eq. (9), the following expressions achieved:

$$M_{zz} = M_{yy} = -\iota^2\left(1 + t_d\frac{\partial}{\partial t}\right)G(r)\frac{\partial\theta(x,t)}{\partial x} \tag{28}$$

$$M_{xx} = 2\iota^2(1 + t_d\frac{\partial}{\partial t})G(r)\frac{\partial\theta(x,t)}{\partial x} \tag{29}$$

$$M_{zx} = M_{xz} = \frac{z}{2}\iota^2\left(1 + t_d\frac{\partial}{\partial t}\right)G(r)\frac{\partial^2\theta(x,t)}{\partial x^2} \tag{30}$$

$$M_{yx} = M_{xy} = -\frac{y}{2}\iota^2\left(1 + t_d\frac{\partial}{\partial t}\right)G(r)\frac{\partial^2\theta(x,t)}{\partial x^2} \tag{31}$$

The remaining components M_{yz} and M_{zy} are equal to zero. Since there is free vibration, the work done by external loads is zero. In the previous sections, the $\acute{\epsilon}$, σ and $\varkappa$ components of viscoelastic nanotubes are achieved. The non-zero component cannot be obtained from Eq. (5). Thus, since $\gamma_z = \gamma_y = \gamma_x = 0$, $P_z = P_y = P_x = 0$. Using Eq. 9, the non-zero components of $\varkappa^*_{ijk}$ are obtained as follows [20]:

$$\varkappa^*_{zzz} = -\frac{y}{5}\frac{\partial^2\theta}{\partial x^2} \tag{32}$$

$$\varkappa^*_{yyy} = \frac{z}{5}\frac{\partial^2\theta}{\partial x^2} \tag{33}$$

$$\varkappa^*_{zzy} = \varkappa^*_{zyz} = \varkappa^*_{yzz} = \frac{y}{15}\frac{\partial^2\theta}{\partial x^2} \tag{34}$$

$$\varkappa^*_{xxz} = \varkappa^*_{zxx} = \varkappa^*_{xzx} = \frac{4y}{15}\frac{\partial^2\theta}{\partial x^2} \tag{35}$$

$$\varkappa^*_{yyz} = \varkappa^*_{zyy} = \varkappa^*_{yzy} = -\frac{y}{15}\frac{\partial^2\theta}{\partial x^2} \tag{36}$$

$$\varkappa^*_{xyx} = \varkappa^*_{yxx} = \varkappa^*_{xxy} = -\frac{4z}{15}\frac{\partial^2\theta}{\partial x^2} \tag{37}$$

The components of T are found with the help of Eq. (6) as follows [20]:

$$T^*_{zzz} = -\frac{2\left(1+t_d\frac{\partial}{\partial t}\right)G(r)\gamma^2 y}{5}\frac{\partial^2\theta}{\partial x^2} \tag{38}$$

$$T^*_{yyy} = \frac{2\left(1+t_d\frac{\partial}{\partial t}\right)G(r)\gamma^2 z}{5}\frac{\partial^2\theta}{\partial x^2} \tag{39}$$

$$T^*_{zzy} = T^*_{zyz} = T^*_{yzz} = \frac{2\left(1+t_d\frac{\partial}{\partial t}\right)G(r)\gamma^2 y}{15}\frac{\partial^2\theta}{\partial x^2} \tag{40}$$

$$T^*_{xxz} = T^*_{zxx} = T^*_{xzx} = \frac{8(1+t_d\frac{\partial}{\partial t})G(r)\gamma^2 y}{15}\frac{\partial^2\theta}{\partial x^2} \tag{41}$$

$$T^*_{yyz} = T^*_{zyy} = T^*_{yzy} = -\frac{2(1+t_d\frac{\partial}{\partial t})G(r)\gamma^2 y}{15}\frac{\partial^2\theta}{\partial x^2} \tag{42}$$

$$T^*_{xyx} = T^*_{yxx} = T^*_{xxy} = -\frac{8\left(1+t_d\frac{\partial}{\partial t}\right)G(r)\gamma^2 z}{15}\frac{\partial^2\theta}{\partial x^2} \tag{43}$$

The strain energy of the nanotube with the components obtained is as follows.

$$U = \frac{1}{2}\int_0^L \left(\begin{array}{l}\left(\left(1+t_d\frac{\partial}{\partial t}\right)GJ + 3\left(1+t_d\frac{\partial}{\partial t}\right)GA\iota^2\right)\left(\frac{\partial\theta}{\partial x}\right)^2 \\ +\left(\frac{8}{15}\left(1+t_d\frac{\partial}{\partial t}\right)GJ\gamma^2 + \frac{1}{4}\left(1+t_d\frac{\partial}{\partial t}\right)GJ\iota^2\right)\left(\frac{\partial^2\theta}{\partial x^2}\right)^2\end{array}\right)dx \tag{44}$$

The kinetic energy of the nanotube is presented as follows:

$$K = \frac{1}{2}\int_0^L\int_A \rho(r)\left[\left(\frac{\partial\psi_x}{\partial t}\right)^2 + \left(\frac{\partial\psi_y}{\partial t}\right)^2 + \left(\frac{\partial\psi_z}{\partial t}\right)^2\right]dAdx = \frac{1}{2}\int_0^L \rho J\left(\frac{\partial\theta}{\partial t}\right)^2 dx \tag{45}$$

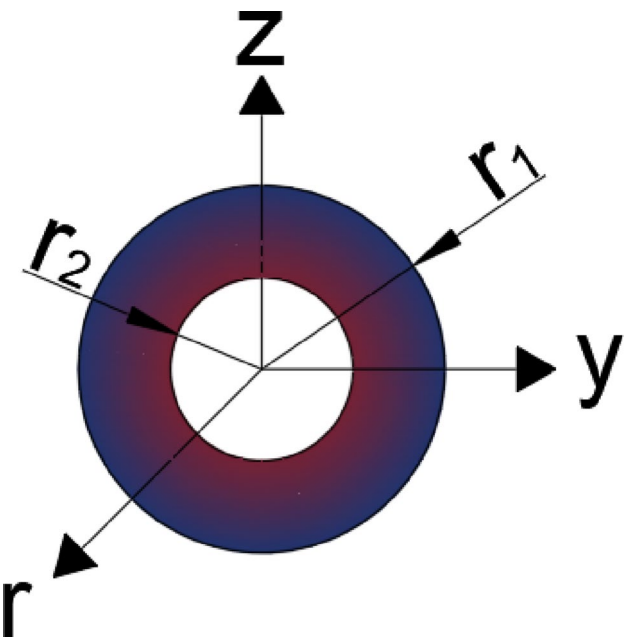


Fig. 1 Cross-section apparent of a FG nanotube

The governing equations can be derived by Hamilton's principle. In the time interval t_1 and t_2, Hamilton's principle is as follows:

$$\delta\int_{t_1}^{t_2}(U-K)\,dt = 0 \tag{46}$$

Here, δ is the variation operator. The governing equations are obtained as follows.

$$\begin{array}{l}-\left(\frac{8}{15}\left(1+t_d\frac{\partial}{\partial t}\right)GJ\gamma^2 + \frac{1}{4}\left(1+t_d\frac{\partial}{\partial t}\right)GJ\iota^2\right)\frac{\partial^4\theta}{\partial x^4} \\ +\left(\begin{array}{l}\left(1+t_d\frac{\partial}{\partial t}\right)GJ \\ +3\left(1+t_d\frac{\partial}{\partial t}\right)GA\iota^2\end{array}\right)\frac{\partial^2\theta}{\partial x^2} - \rho J\frac{\partial^2\theta}{\partial t^2} = 0\end{array} \tag{47}$$

$$\begin{array}{l}\left(\frac{8}{15}\left(1+t_d\frac{\partial}{\partial t}\right)GJ\gamma^2 + \frac{1}{4}\left(1+t_d\frac{\partial}{\partial t}\right)GJ\iota^2\right)\frac{\partial^3\theta}{\partial x^3} \\ -\left(\begin{array}{l}\left(1+t_d\frac{\partial}{\partial t}\right)GJ \\ +3\left(1+t_d\frac{\partial}{\partial t}\right)GA\iota^2\end{array}\right)\frac{\partial\theta}{\partial x} = 0\ or\ \delta\theta = 0\end{array} \tag{48}$$

$$\left(\begin{array}{l}\frac{8}{15}\left(1+t_d\frac{\partial}{\partial t}\right)GJ\gamma^2 \\ +\frac{1}{4}\left(1+t_d\frac{\partial}{\partial t}\right)GJ\iota^2\end{array}\right)\frac{\partial^2\theta}{\partial x^2} = 0\ or\ \delta\frac{\partial\theta}{\partial x} = 0 \tag{49}$$

When the governing equation is analyzed, it is noticed that ζ, one of the three material length scale parameters, has no effect on torsional vibration. The material length scale parameters that affect the torsional vibration are γ and ι. Moreover, when γ = 0, the governing equation and boundary conditions are transformed into the governing equations for MCST. Furthermore, the values of the length scale parameters of the material used in this study have been determined by considering the ranges reported in similar studies in literature.

Functionally graded nanotubes (FGNTs) are a class of advanced materials whose properties vary continuously across the radial direction, allowing for improved performance and tailored behavior in various applications. In FGNTs, material properties such as modulus of elasticity, shear modulus, density, and thermal conductivity are

smoothly distributed according to a predefined gradient. This gradient typically follows a power-law or exponential distribution depending on the volume fractions of the constituent materials. In this study, the tube's cross-section, shown in Fig. 1, will undergo functional grading. The mechanical properties of the nanotube will be determined using the equation provided in reference [25].

$$P(r) = P_s \Pi_s + P_a \Pi_a \tag{50}$$

Where P_s and P_a represent the properties of the FG nanotube's inner and outer surfaces, respectively. Similarly, Π_s and Π_a denote the volume fractions of silicon and aluminum, which are the materials considered in this analysis. These parameters are related by the following equation:

$$\Pi_s + \Pi_a = 1 \tag{51}$$

The volume fraction Π_s is expressed as:

$$\Pi_s = \left(\frac{r - r_2}{r_1 - r_2}\right)^k \tag{52}$$

Here, k is the power-law exponent, a positive value that governs the variation of material properties through the thickness of the nanotube. When $k = 0$, the material consists entirely of silicon. Conversely, as k becomes very large, the material approaches pure aluminum. Based on this, material parameters such as modulus of elasticity (E), Poisson's ratio (μ), and density (ρ) vary according to the following relations.

$$E(r) = (E_s - E_a)\left(\frac{r - r_2}{r_1 - r_2}\right)^k + E_a \tag{53}$$

$$\mu(r) = (\mu_s - \mu_a)\left(\frac{r - r_2}{r_1 - r_2}\right)^k + \mu_a \tag{54}$$

$$\rho(r) = (\rho_s - \rho_a)\left(\frac{r - r_2}{r_1 - r_2}\right)^k + \rho_a \tag{55}$$

As a result of this functional grading process, some effects on the equations of motion will be as follows.

$$GJ = 2\pi \int_{r_2}^{r_1} G(r)\, r^3 dr \tag{56}$$

$$GA = 2\pi \int_{r_2}^{r_1} G(r)\, r dr \tag{57}$$

$$\bar{\rho}^J = 2\pi \int_{r_2}^{r_1} \rho\ (r)\, r^3 dr \tag{58}$$

3 Solution of problem

In this section, a general solution for torsional vibration of a viscoelastic strain gradient nanotube under viscoelastic boundary conditions will be presented. Before proceeding to the solution stage, the functions of 2 variables depending on time and position will be converted into a function of one variable depending on position using the equation below.

$$\theta\ (x,t) = \theta\ (x)\, e^{i\omega t} \tag{59}$$

If the above equation is substituted into the governing equation, it is obtained as follows.

$$-\left(\begin{matrix}\frac{8}{15}\bar{\mu}^J \gamma^2 \\ +\frac{1}{4}\bar{\mu}^J \iota^2\end{matrix}\right)\frac{d^4\theta\ (x)}{dx^4} + \left(\begin{matrix}\bar{\mu}^J \\ +3\bar{\mu}^A \iota^2\end{matrix}\right)\frac{d^2\theta\ (x)}{dx^2} + \omega^2 \bar{\rho}^J \theta\ (x) = 0 \tag{60}$$

Here, $\bar{\mu}^A$ and $\bar{\mu}^J$ are defined by:

$$\bar{\mu}^J = (1 + i\omega\, t_d)\, GJ \tag{61}$$

$$\bar{\mu}^A = (1 + i\omega\, t_d)\, GA \tag{62}$$

Here ω is the angular frequency and θ is the rotation function. As indicated in the governing equation, there are 2 scale parameters. If the γ is equal to zero, results for MCST are obtained. In this study, the Fourier Sine series of rotation function is chosen for the solution of the problem as follows.

$$\theta\ (x) = \sum_{n=1}^{\infty} A_n sin\,(\beta\, x);\ \ \beta = \frac{n\pi}{L} \tag{63}$$

Where A_n is the Fourier coefficient. The higher order derivatives of the rotation function are obtained with the aid of Stokes transforms and are presented below [26].

$$\frac{d\theta(x)}{dx} = \frac{\theta_L - \theta_0}{L} + \sum_{n=1}^{\infty}\left(\frac{2\left((-1)^n\theta_L - \theta_0\right)}{L} + \beta A_n\right)\cos(\beta x) \tag{64}$$

$$\frac{d^2\theta(x)}{dx^2} = -\sum_{n=1}^{\infty}\beta\left(\frac{2\left((-1)^n\theta_L - \theta_0\right)}{L} + \beta A_n\right)\sin(\beta x) \tag{65}$$

$$\frac{d^3\theta(x)}{dx^3} = \frac{\theta_L'' - \theta_0''}{L} + \sum_{n=1}^{\infty}\begin{pmatrix}\frac{2\left((-1)^n\theta_L'' - \theta_0''\right)}{L}\\ -\beta^2\left(\frac{2\left((-1)^n\theta_L - \theta_0\right)}{L} + \beta A_n\right)\end{pmatrix}\cos(\beta x) \tag{66}$$

$$\frac{d^4\theta(x)}{dx^4} = -\sum_{n=1}^{\infty}\beta\begin{pmatrix}\frac{2\left((-1)^n\theta_L'' - \theta_0''\right)}{L}\\ -\beta^2\left(\frac{2\left((-1)^n\theta_L - \theta_0\right)}{L} + \beta A_n\right)\end{pmatrix}\sin(\beta x) \tag{67}$$

By substituting the above functions in the governing equation, the Fourier coefficient is determined as follows.

$$A_n = \frac{\begin{matrix}2n\pi\,\theta_0(180\iota^2\bar{\mu}^A L^2 \\ +H_a\bar{\mu}^J)\end{matrix}}{\begin{matrix}(n^4\pi^4 H_b \\ +60n^2\pi^2L^2)\bar{\mu}^J - 60L^2H_b\end{matrix}} - \frac{\begin{matrix}2(-1)^n n\pi\,\theta_L(180\iota^2\bar{\mu}^A L^2 \\ +H_a\bar{\mu}^J)\end{matrix}}{\begin{matrix}(n^4\pi^4 H_b \\ +60n^2\pi^2L^2)\bar{\mu}^J - 60L^2H_b\end{matrix}} \tag{68}$$

In which, H_a and H_b are written by:

$$H_a = \pi^2n^2\left(32\gamma^2 + 15\iota^2\right) + 60L^2 \tag{69}$$

$$H_b = L^2\overline{\rho^J}\omega^2 - 3n^2\pi^2\overline{\mu^A}\iota^2 \tag{70}$$

Figure 2 displays the viscoelastic boundary conditions of a nanotube. Kelvin Voigt model has been used for viscoelastic boundary conditions. In the figure, K_0 and K_L represent spring constants while C_0 and C_L represent viscosity. Thanks to this model, the beam can be evaluated separately in both elastic and viscous boundary conditions. If the spring constants are chosen to be zero, viscous boundary conditions occur, and if the viscosity is chosen to be zero, elastic boundary conditions occur. In the literature, results for rigid boundary conditions are often presented. Thanks to this method, results for elastic and viscous boundary conditions can be found separately, and results for viscoelastic boundary conditions can also be found.

The solution of this problem is realized for viscoelastic boundary conditions using the following equations. Qiao and Rahmatalla [56] also provided viscoelastic boundary conditions in this manner.

$$x = 0 \rightarrow \begin{pmatrix}\frac{8}{15}\overline{\mu^J}\gamma^2\\ +\frac{1}{4}\overline{\mu^J}\iota^2\end{pmatrix}\frac{\partial^3\theta}{\partial x^3} - \left(\overline{\mu^J} + 3\overline{\mu^A}\iota^2\right)\frac{\partial\theta}{\partial x} = K\theta + C\frac{\partial\theta}{\partial t} \tag{71}$$

$$x = L \rightarrow \begin{pmatrix}\frac{8}{15}\overline{\mu^J}\gamma^2\\ +\frac{1}{4}\overline{\mu^J}\iota^2\end{pmatrix}\frac{\partial^3\theta}{\partial x^3} - \left(\overline{\mu^J} + 3\overline{\mu^A}\iota^2\right)\frac{\partial\theta}{\partial x} = -K\theta - C\frac{\partial\theta}{\partial t} \tag{72}$$

If the above equations are organized depending on the position, they are obtained as follows.

$$\begin{pmatrix}\frac{8}{15}\overline{\mu^J}\gamma^2\\ +\frac{1}{4}\overline{\mu^J}\iota^2\end{pmatrix}\frac{\partial^3\theta}{\partial x^3} - \left(\overline{\mu^J} + 3\overline{\mu^A}\iota^2\right)\frac{\partial\theta}{\partial x}|_{x=0} = K_0\theta_0 + i\omega C_0\theta_0 \tag{73}$$

$$\begin{pmatrix}\frac{8}{15}\overline{\mu^J}\gamma^2\\ +\frac{1}{4}GJ\iota^2\end{pmatrix}\frac{\partial^3\theta}{\partial x^3} - \left(\overline{\mu^J} + 3\overline{\mu^A}\iota^2\right)\frac{\partial\theta}{\partial x}|_{x=L} = -K_L\theta_L - i\omega C_L\theta_L \tag{74}$$

In the equations K_0 and K_L represent spring constants and C_0 and C_L represent viscosity. The above two equations are written in matrix form as follows.

$$\begin{bmatrix} M_{11} & M_{12} \\ M_{21} & M_{22}\end{bmatrix}\begin{bmatrix}\theta_0 \\ \theta_L\end{bmatrix} = 0 \tag{75}$$

To calculate the angular frequencies, the determinant of the above 2×2 matrix must be taken and set equal to zero as follows.

$$\begin{vmatrix} M_{11} & M_{12} \\ M_{21} & M_{22}\end{vmatrix} = 0 \tag{76}$$

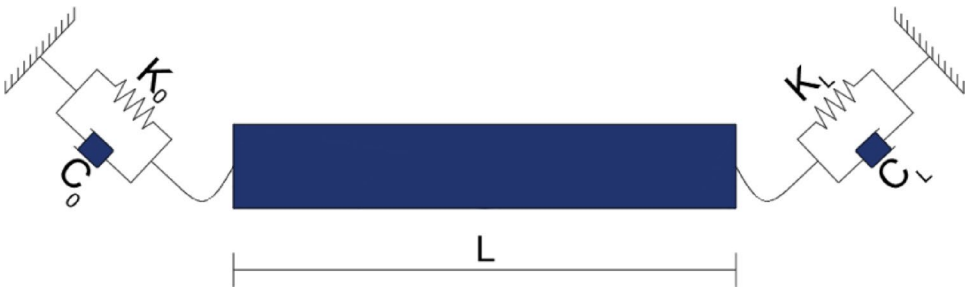


Fig. 2 A strain gradient viscoelastic nanotube restrained with Kelvin Voigt viscoelastic model

Table 1 Material properties of the viscoelastic FG nanotube

Material	Elasticity Modul (E)	Poisson Ratio (μ)	Bulk mass density (ρ)
Silicon	210 GPa	0.24	2331 kg/m3
Aluminum	68.5 GPa	0.35	2700 kg/m3

The components of the above matrix are defined by:

$$M_{11} = -i\omega C_0 - K_0 - \frac{\bar{\mu}^J}{L} - \frac{3\iota^2\bar{\mu}^A}{L} - \sum_{n=1}^{\infty} \frac{L\left(\begin{matrix}180\iota^2L^2\bar{\mu}^A\\+\bar{\mu}^J H_a\end{matrix}\right)\bar{\rho}^J\omega^2}{60\left(\begin{matrix}\omega^2L^2\bar{\rho}^J\\-3n^2\pi^2\iota^2\bar{\mu}^A\end{matrix}\right)L^2 - \left(\begin{matrix}60n^2\pi^2L^2\\+n^4\pi^4H_b\end{matrix}\right)\bar{\mu}^J} \tag{77}$$

$$M_{12} = \frac{\bar{\mu}^J}{L} + \frac{3\iota^2\bar{\mu}^A}{L} + \sum_{n=1}^{\infty} \frac{2(-1)^n L\left(\begin{matrix}180\iota^2L^2\bar{\mu}^A\\+\bar{\mu}^J H_a\end{matrix}\right)\bar{\rho}^J\omega^2}{60\left(\begin{matrix}\omega^2L^2\bar{\rho}^J\\-3n^2\pi^2\iota^2\bar{\mu}^A\end{matrix}\right)L^2 - \left(\begin{matrix}60n^2\pi^2L^2\\+n^4\pi^4H_b\end{matrix}\right)\bar{\mu}^J} \tag{78}$$

$$M_{21} = \frac{\bar{\mu}^J}{L} + \frac{3\iota^2\bar{\mu}^A}{L} + \sum_{n=1}^{\infty} \frac{2(-1)^n L\left(\begin{matrix}180\iota^2L^2\bar{\mu}^A\\+\bar{\mu}^J H_a\end{matrix}\right)\bar{\rho}^J\omega^2}{60\left(\begin{matrix}\omega^2L^2\bar{\rho}^J\\-3n^2\pi^2\iota^2\bar{\mu}^A\end{matrix}\right)L^2 - \left(\begin{matrix}60n^2\pi^2L^2\\+n^4\pi^4H_b\end{matrix}\right)\bar{\mu}^J} \tag{79}$$

$$M_{22} = -i\omega C_L - K_L - \frac{\bar{\mu}^J}{L} - \frac{3\iota^2\bar{\mu}^A}{L} - \sum_{n=1}^{\infty} \frac{L\left(\begin{matrix}180\iota^2L^2\bar{\mu}^A\\+\bar{\mu}^J H_a\end{matrix}\right)\bar{\rho}^J\omega^2}{60\left(\begin{matrix}\omega^2L^2\bar{\rho}^J\\-3n^2\pi^2\iota^2\bar{\mu}^A\end{matrix}\right)L^2 - \left(\begin{matrix}60n^2\pi^2L^2\\+n^4\pi^4H_b\end{matrix}\right)\bar{\mu}^J} \tag{80}$$

The above equations are the most general solution for the torsional vibration of nanotubes with nanoscale strain gradient including viscous damping coefficient, material length scale parameters in viscoelastic boundary conditions. When the viscous damping coefficient is zero, the angular frequencies of torsional vibration of nanotubes without damping effect can be obtained, while for viscous damping coefficient values other than zero, the effect of damping will be reflected on the angular frequency. As mentioned before, when $\gamma = 0$, the results are also obtained for MCST. The semi-analytical solution method presented in this study is preferred because it has many advantages. The most important one is that this method allows the torsional vibration analysis of nanotubes with viscoelastic strain gradient to be performed under viscoelastic boundary conditions. There are very limited studies in literature using these boundary conditions. In addition, thanks to the model used, these boundary conditions can be transformed into elastic boundary conditions as well as rigid boundary conditions.

4 Results and discussion

In this section, results and discussion on the torsional vibration of a strain gradient viscoelastic nanotube are presented. To enforce rigid boundary conditions, $k = 10^9$ (spring constant) $c = 0$ (viscosity) has been chosen, and the solution has been performed with 20 terms. The properties in Table 1 have been used as material properties [9]. Geometric properties are $r_1 = Ro = 2$, $r_2 = 1$ and $L/r_1 = 10$ unless otherwise stated.

While presenting the results, some dimensionlessization has been done. The non-dimensional frequency (λ) and viscous damping parameter (τ) are presented below.

$$\lambda = \omega L\sqrt{\frac{\rho_s}{G_s}} \tag{81}$$

$$\tau = \frac{t_d}{L\sqrt{\frac{\rho_s}{G_s}}} \tag{82}$$

Table 2 Comparison of λ values for various mode numbers

ι=γ	Equation (83)					In this work $N=20$				
	λ1	λ2	λ3	λ4	λ5	λ1	λ2	λ3	λ4	λ5
0	3.142	6.283	9.425	12.566	15.708	3.142	6.283	9.425	12.566	15.708
0.5	3.589	7.217	10.924	14.748	18.723	3.589	7.217	10.924	14.748	18.724
1	4.680	9.482	14.521	19.906	25.730	4.680	9.482	14.521	19.906	25.730
1.5	6.078	12.367	19.064	26.347	34.369	6.078	12.367	19.064	26.347	34.369
2	7.616	15.530	24.021	33.335	43.681	7.616	15.530	24.021	33.335	43.681
2.5	9.224	18.832	29.182	40.589	53.315	9.224	18.832	29.182	40.589	53.315

Table 3 Variation of non-dimensional frequencies depending on the viscous damping parameter and scale parameters

B.C.	τ	γ=0						γ=1					
		ι=0			ι=0.5			ι=0			ι=0.5		
		λ1	λ2	λ3	λ1	λ2	λ3	λ1	λ2	λ3	λ1	λ2	λ3
C-C	0	2.681	5.361	8.042	3.022	6.056	9.111	2.698	5.501	8.505	3.038	6.179	9.522
	0.01	2.68+0.036i	5.36+0.144i	8.036+0.323i	3.022+0.046i	6.053+0.183i	9.101+0.415i	2.698+0.036i	5.499+0.151i	8.497+0.362i	3.038+0.046i	6.176+0.191i	9.511+0.453i
	0.02	2.68+0.072i	5.354+0.287i	8.016+0.647i	3.021+0.091i	6.044+0.367i	9.073+0.83i	2.697+0.073i	5.492+0.303i	8.474+0.723i	3.037+0.092i	6.167+0.382i	9.479+0.907i
	0.03	2.679+0.108i	5.344+0.431i	7.983+0.97i	3.019+0.137i	6.031+0.55i	9.025+1.245i	2.696+0.109i	5.482+0.454i	8.436+1.085i	3.035+0.138i	6.153+0.573i	9.424+1.36i
	0.04	2.677+0.144i	5.331+0.575i	7.937+1.294i	3.017+0.183i	6.011+0.733i	8.958+1.66i	2.694+0.146i	5.467+0.605i	8.381+1.447i	3.032+0.185i	6.132+0.764i	9.348+1.813i
	0.05	2.675+0.18i	5.313+0.719i	7.878+1.617i	3.014+0.228i	5.986+0.917i	8.871+2.075i	2.692+0.182i	5.448+0.756i	8.311+1.808i	3.029+0.231i	6.105+0.955i	9.248+2.267i
	0.06	2.672+0.216i	5.292+0.862i	7.805+1.94i	3.01+0.274i	5.955+1.1i	8.764+2.49i	2.689+0.218i	5.425+0.908i	8.224+2.17i	3.025+0.277i	6.072+1.145i	9.125+2.72i
	0.07	2.669+0.252i	5.266+1.006i	7.717+2.264i	3.005+0.32i	5.918+1.283i	8.635+2.905i	2.686+0.255i	5.398+1.059i	8.119+2.532i	3.021+0.323i	6.033+1.336i	8.978+3.173i
	0.08	2.665+0.287i	5.237+1.15i	7.615+2.587i	3+0.365i	5.875+1.467i	8.484+3.32i	2.683+0.291i	5.366+1.21i	7.998+2.893i	3.015+0.369i	5.988+1.527i	8.804+3.627i
	0.09	2.661+0.323i	5.203+1.294i	7.497+2.91i	2.994+0.411i	5.826+1.65i	8.31+3.735i	2.678+0.328i	5.33+1.362i	7.857+3.255i	3.009+0.415i	5.936+1.718i	8.604+4.08i
	0.1	2.657+0.359i	5.165+1.437i	7.363+3.234i	2.988+0.457i	5.771+1.834i	8.111+4.15i	2.674+0.364i	5.289+1.513i	7.698+3.617i	3.003+0.461i	5.877+1.909i	8.374+4.533i
C-F	0	1.34	4.021	6.702	1.51	4.537	7.58	1.343	4.08	6.972	1.512	4.589	7.82
	0.01	1.34+0.009i	4.02+0.081i	6.698+0.225i	1.51+0.011i	4.536+0.103i	7.574+0.287i	1.343+0.009i	4.079+0.083i	6.968+0.243i	1.512+0.011i	4.588+0.105i	7.814+0.306i
	0.02	1.34+0.018i	4.018+0.162i	6.687+0.449i	1.51+0.023i	4.532+0.206i	7.558+0.575i	1.342+0.018i	4.077+0.166i	6.955+0.486i	1.512+0.023i	4.585+0.211i	7.796+0.611i
	0.03	1.34+0.027i	4.014+0.243i	6.668+0.674i	1.51+0.034i	4.526+0.309i	7.531+0.862i	1.342+0.027i	4.073+0.25i	6.934+0.729i	1.512+0.034i	4.578+0.316i	7.766+0.917i
	0.04	1.34+0.036i	4.008+0.323i	6.641+0.898i	1.51+0.046i	4.518+0.412i	7.492+1.149i	1.342+0.036i	4.067+0.333i	6.904+0.972i	1.512+0.046i	4.57+0.421i	7.723+1.223i
	0.05	1.34+0.045i	4.001+0.404i	6.607+1.123i	1.509+0.057i	4.508+0.515i	7.442+1.436i	1.342+0.045i	4.059+0.416i	6.865+1.215i	1.511+0.057i	4.559+0.527i	7.669+1.529i
	0.06	1.339+0.054i	3.992+0.485i	6.565+1.347i	1.509+0.068i	4.495+0.618i	7.381+1.724i	1.341+0.054i	4.049+0.499i	6.818+1.458i	1.511+0.069i	4.546+0.632i	7.601+1.834i
	0.07	1.339+0.063i	3.981+0.566i	6.515+1.572i	1.508+0.08i	4.479+0.72i	7.308+2.011i	1.341+0.063i	4.038+0.583i	6.761+1.701i	1.51+0.08i	4.53+0.737i	7.521+2.14i
	0.08	1.338+0.072i	3.969+0.647i	6.456+1.797i	1.508+0.091i	4.462+0.823i	7.223+2.298i	1.341+0.072i	4.025+0.666i	6.695+1.944i	1.51+0.091i	4.511+0.842i	7.427+2.446i
	0.09	1.338+0.081i	3.955+0.728i	6.39+2.021i	1.507+0.103i	4.441+0.926i	7.125+2.585i	1.34+0.081i	4.011+0.749i	6.62+2.187i	1.509+0.103i	4.49+0.948i	7.32+2.752i
	0.1	1.337+0.09i	3.939+0.808i	6.314+2.246i	1.506+0.114i	4.419+1.029i	7.014+2.873i	1.34+0.09i	3.994+0.832i	6.535+2.43i	1.508+0.114i	4.467+1.053i	7.197+3.057i

Table 4 Variation of non-dimensional frequencies depending on the power-law exponent

k	C-C			C-F		
	λ1	λ2	λ3	λ1	λ2	λ3
0	4.67888 + 0.10952i	9.47115 + 0.44952i	14.48303 + 1.05435i	2.33227 + 0.0272i	7.05395 + 0.2491i	11.94346 + 0.71579i
0.2	4.45653 + 0.09935i	9.02446 + 0.40804i	13.8083 + 0.95793i	2.22122 + 0.02467i	6.7198 + 0.22603i	11.38331 + 0.65001i
0.5	4.19424 + 0.088i	8.49622 + 0.36158i	13.00718 + 0.84954i	2.09031 + 0.02185i	6.32521 + 0.20024i	10.71967 + 0.57622i
1	3.88168 + 0.07537i	7.86532 + 0.3098i	12.04691 + 0.72829i	1.9344 + 0.01871i	5.85455 + 0.17153i	9.92575 + 0.49382i
2	3.50371 + 0.0614i	7.10087 + 0.25243i	10.87971 + 0.5936i	1.74595 + 0.01524i	5.28491 + 0.13975i	8.9624 + 0.40243i
5	3.03314 + 0.04601i	6.1475 + 0.18914i	9.42002 + 0.44467i	1.51144 + 0.01142i	4.57521 + 0.10472i	7.75946 + 0.3015i
10	2.77155 + 0.03842i	5.61677 + 0.15787i	8.60559 + 0.37097i	1.38112 + 0.00954i	4.18045 + 0.08742i	7.0891 + 0.25159i
20	2.59971 + 0.0338i	5.26773 + 0.13884i	8.06899 + 0.32608i	1.29555 + 0.00839i	3.92101 + 0.0769i	6.64786 + 0.22122i

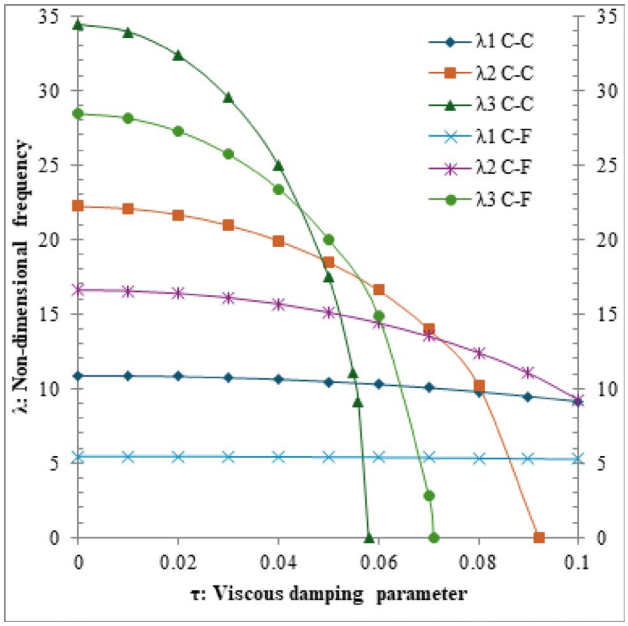


Fig. 3 Variation of real values of non-dimensional frequencies in the first 3 modes for different boundary conditions depending on the viscous damping parameter

In order to verify the accuracy of the results, the following equation, which is available in the literature, has been used. This equation provides the calculation of the angular frequencies of a strain gradient nanotube under C-C (Clamped-Clamped) boundary conditions [20].

$$\omega = \frac{\pi m}{L}\sqrt{\frac{GJ\left(\frac{m\pi}{L}\right)^2\left(\frac{1}{4}\iota^2+\frac{8}{15}\gamma^2\right)+G\left(J+3A\iota^2\right)}{\rho J}} \tag{83}$$

Using this equation, the comparison in Table 2 has been built. As can be displayed, the results are satisfactory. Additionally, it is thought that since the scale parameters increase stiffness, the frequency values also increase as the scale parameters increase.

In addition, the variation of the non-dimensional frequencies of a nanotube with viscoelastic strain gradient depending on the viscous damping parameter at various scale parameter values (ι and γ) in C-C (clamped-clamped) and C-F (clamped-free) boundary conditions are displayed in Table 3. As can be observed, when τ = 0, non-dimensional frequencies take real values, while when τ > 0, frequencies appear as complex numbers as the sum of real and imaginary values. The results of the changes in these values have been evaluated by converting the results into graphs and analyzing them separately as real and imaginary values. In addition, the relationships between real and imagined values have been also revealed.

When Navier type solution methods are employed, exact solutions of the dimensionless frequencies for viscoelastic nanotubes are found as follows.

$$\lambda_{C-C} = \left(\frac{\left(\left(GJ+3GA\iota^2\right)\left(\frac{\pi m}{L}\right)^2 + \left(\frac{8}{15}GJ\gamma^2+\frac{1}{4}GJ\iota^2\right)\left(\frac{\pi m}{L}\right)^4\right)t_d}{2\rho J} i + \frac{\sqrt{-\left(\left(\left(GJ+3GA\iota^2\right)\left(\frac{\pi m}{L}\right)^2 + \left(\frac{8}{15}GJ\gamma^2+\frac{1}{4}GJ\iota^2\right)\left(\frac{\pi m}{L}\right)^4\right)t_d\right)^2 + 4\rho J\left(\left(GJ+3GA\iota^2\right)\left(\frac{\pi m}{L}\right)^2 + \left(\frac{8}{15}GJ\gamma^2+\frac{1}{4}GJ\iota^2\right)\left(\frac{\pi m}{L}\right)^4\right)}}{2\rho J} \right) L\sqrt{\frac{\rho}{G}} \tag{84}$$

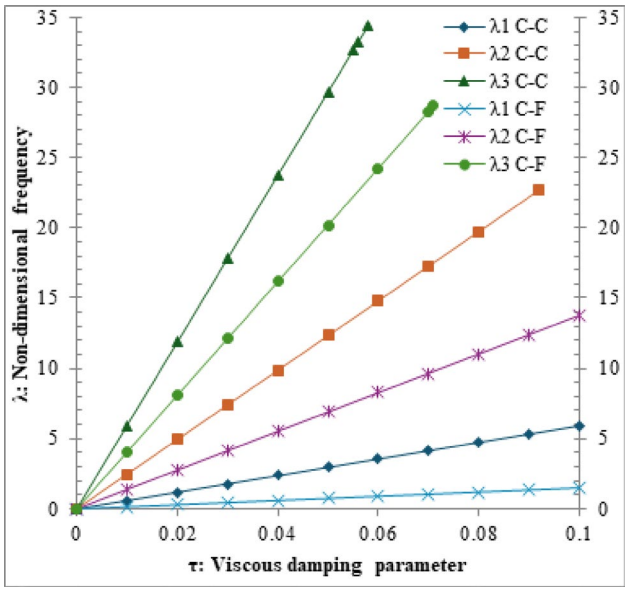


Fig. 4 Variation of imaginary values of non-dimensional frequencies in the first 3 modes for different boundary conditions depending on the viscous damping parameter

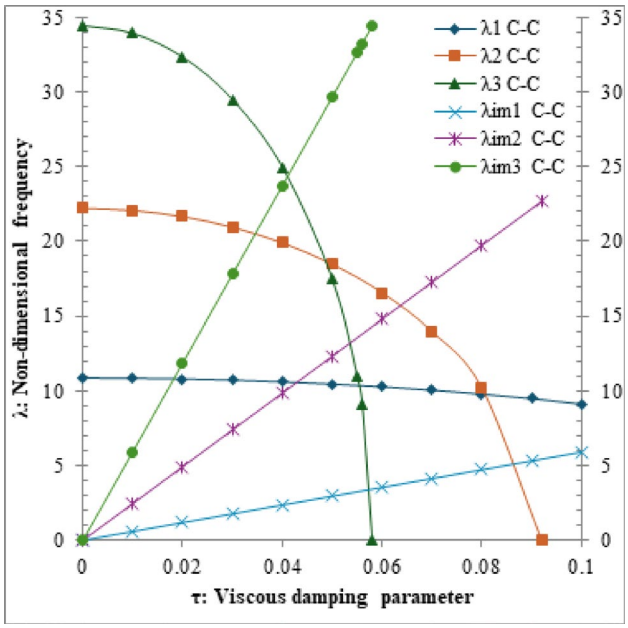


Fig. 5 Variation of real and imaginary values of non-dimensional frequencies in the first 3 modes for C-C boundary conditions depending on the viscous damping parameter

$$\lambda_{C-F}=\left(\frac{\left(\left(GJ+3GA\iota^2\right)\left(\frac{(2m-1)\pi}{2L}\right)^2+\left(\frac{8}{15}GJ\gamma^2+\frac{1}{4}GJ\iota^2\right)\left(\left(\frac{(2m-1)\pi}{2L}\right)\right)^4\right)t_d}{2\rho J}i+\frac{\sqrt{-\left(\left(\left(GJ+3GA\iota^2\right)\left(\left(\frac{(2m-1)\pi}{2L}\right)\right)^2+\left(\frac{8}{15}GJ\gamma^2+\frac{1}{4}GJ\iota^2\right)\left(\left(\frac{(2m-1)\pi}{2L}\right)\right)^4\right)t_d\right)^2+4\rho J\left(\left(GJ+3GA\iota^2\right)\left(\left(\frac{(2m-1)\pi}{2L}\right)\right)^2+\left(\frac{8}{15}GJ\gamma^2+\frac{1}{4}GJ\iota^2\right)\left(\left(\frac{(2m-1)\pi}{2L}\right)\right)^4\right)}}{2\rho J}\right)L\sqrt{\frac{\rho}{G}} \tag{85}$$

Where m is the number of modes. If these close solutions are compared with the tables presented, it will be observed that the results are in agreement with each other.

Table 4 presents the variation of torsional vibration frequencies of viscoelastic nanotubes as a function of the k. As can be noticed in the table, the real values of the dimensionless frequencies decrease as the k rises. This is because the material changes from one material to another with increasing the k. In other words, with the increment of k, the parameter affecting the stiffness such as modulus of elasticity and the parameter affecting the mass such as density change. Therefore, depending on the increase in k, the frequency changes depending on the change in the modulus of elasticity and density of the material.

Figure 3 illustrates the variation of the real values of the non-dimensional frequencies as a function of the viscous damping parameter in the first 3 modes for C-C and C-F boundary conditions. In the graph, it is visible that as the viscous damping parameter grows, the large modes diminish and overtake the small modes. Similar results have also been observed by Eltaher et al. [7]. Therefore, imaginary values should be considered when determining the number of a mode under damping effect. It will be realized that the ordering of the imaginary values from small to large will yield the order of the modes. As can be noticed from the graph, since λ3 C-C decreases more than λ3 C-F and is zero for a smaller value of the viscous damping parameter, the damping effect is larger for more rigid boundary conditions. Vibration occurs more rapidly under more rigid boundary

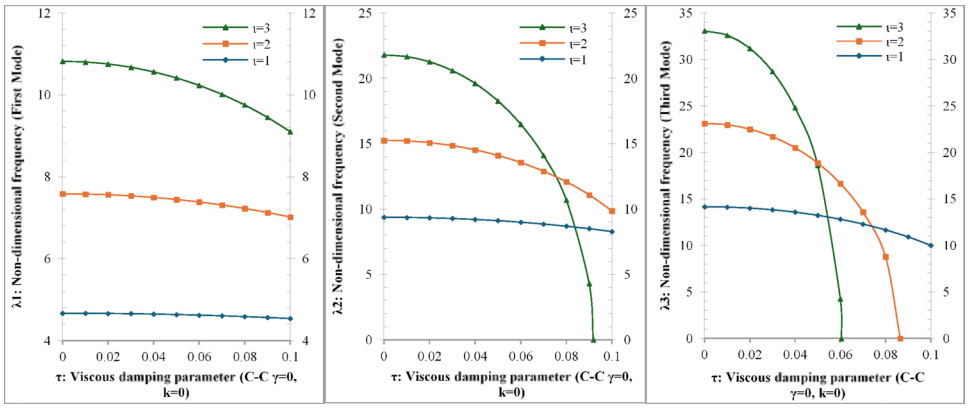


Fig. 6 Variation of real values of non-dimensional frequencies depending on the viscous damping parameter at different scale parameters

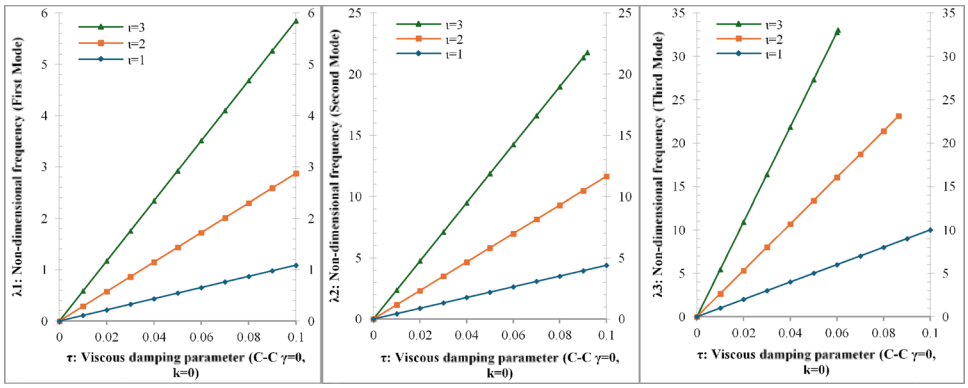


Fig. 7 Variation of imaginary values of non-dimensional frequencies depending on the viscous damping parameter at different scale parameters

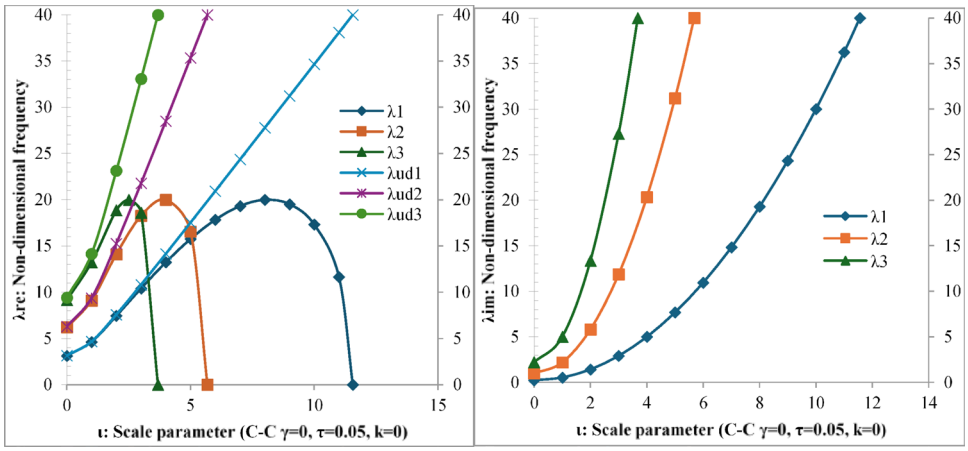


Fig. 8 Variation of real and imaginary values of the non-dimensional frequencies of a CNT with constant viscous damping parameter depending on the scale parameter

conditions. Therefore, it is thought that damping is more effective under more rigid boundary conditions due to its variation with speed. Moreover, the effect of the viscous damping parameter is larger for large modes. This may be because damping changes with speed, so vibration speed is higher in high modes, making damping more effective in large modes.

Figure 4 displays the variation of the imaginary values of the non-dimensional frequencies for the C-C and C-F boundary conditions for the first 3 modes. As the viscous damping parameter rises, the imaginary values of the non-dimensional frequencies tend to increase linearly. These lines terminate at the points where the real values are zero. It is believed that the slopes of these lines affect the damping capacity. Thus, the greater the slope, the greater the effect of damping on the frequency. Zhen et al. [15] have also stated that the imaginary values of the dimensionless frequencies change linearly as the viscous damping parameter increases.

Figure 5 presents on a single graph the variation of imaginary and real values of the non-dimensional frequencies for the C-C boundary conditions for the first 3 modes with respect to the viscous damping parameter. The non-dimensional frequencies (λ) of a damped beam are expressed as

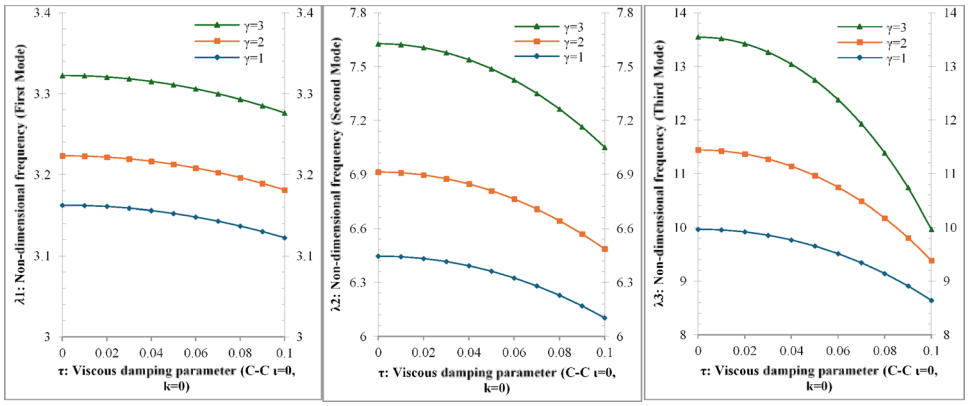


Fig. 9 Variation of real values of non-dimensional frequencies depending on the viscous damping parameter at different scale parameters

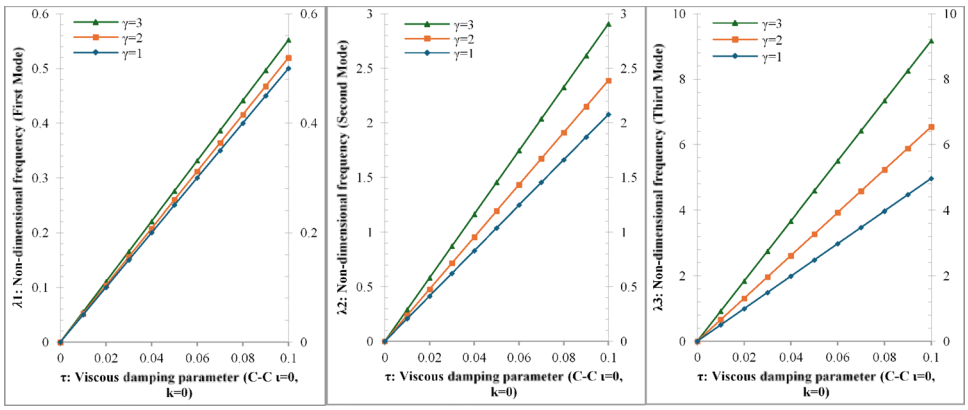


Fig. 10 Variation of imaginary values of non-dimensional frequencies depending on the viscous damping parameter at different scale parameters

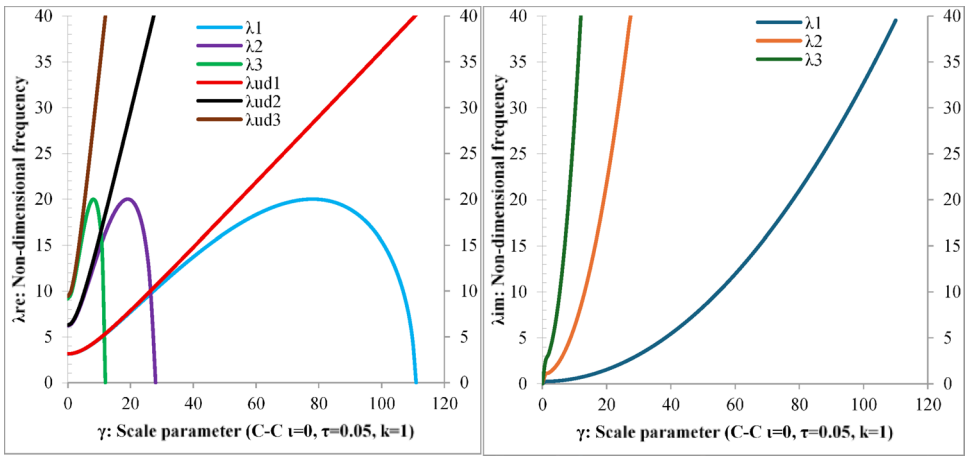


Fig. 11 Variation of real and imaginary values of the non-dimensional frequencies of a CNT with constant viscous damping parameter depending on the scale parameter

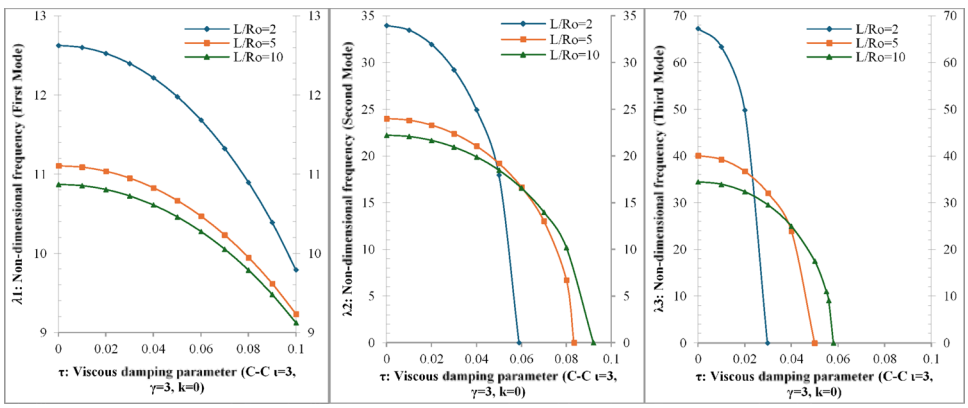


Fig. 12 Variation of real values of non-dimensional frequencies at different L/Ro values depending on the viscous damping parameter

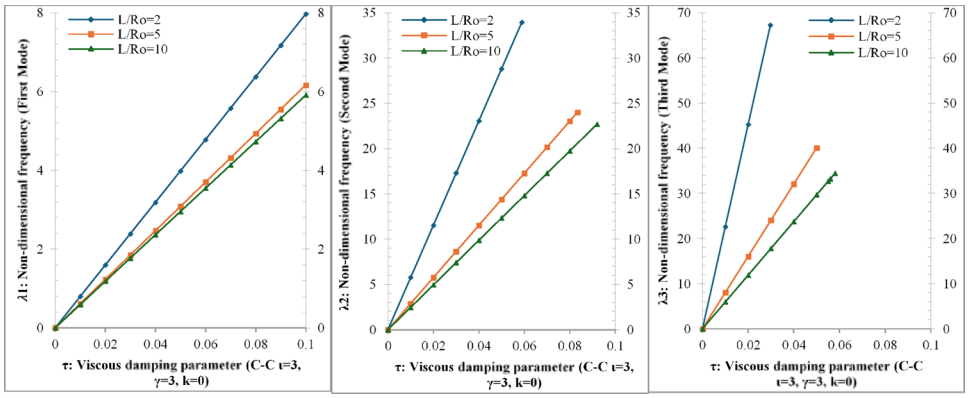


Fig. 13 Variation of imaginary values of non-dimensional frequencies at different L/Ro values depending on the viscous damping parameter

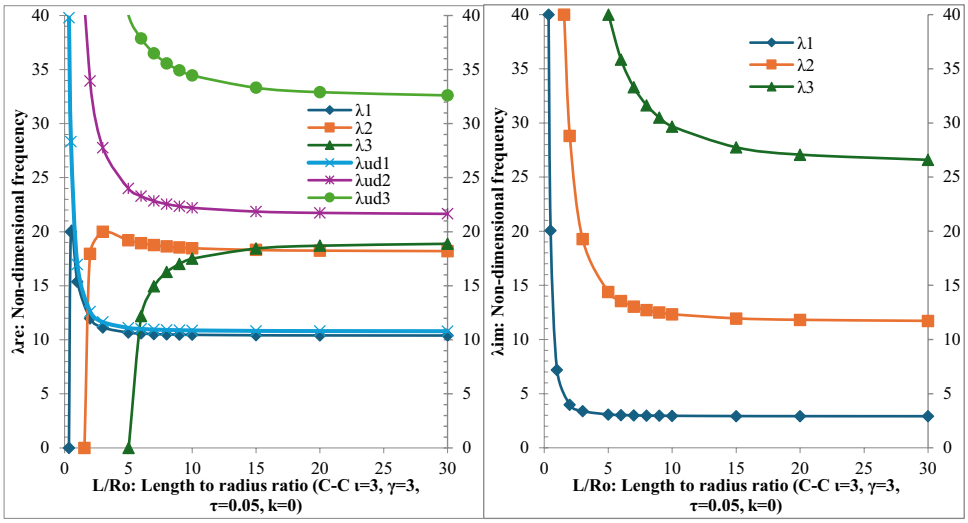


Fig. 14 Variation of real and imaginary values of the non-dimensional frequencies of a CNT with a constant viscous damping parameter depending on L/Ro

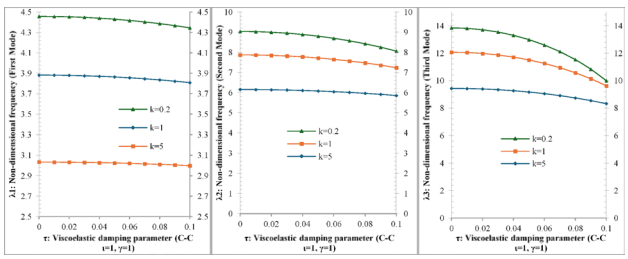


Fig. 15 Variation of real values of non-dimensional frequencies depending on the viscous damping parameter at different power-law exponents

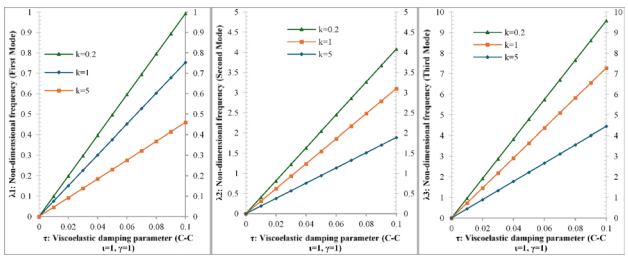


Fig. 16 Variation of imaginary values of non-dimensional frequencies depending on the viscous damping parameter at different power-law exponents

the sum of the real (λre) and imaginary (λim) values as follows.

$$\lambda = \lambda_{re} + \lambda_{im} \tag{86}$$

If the imaginary values are zero, i.e. the viscous damping parameter is zero, the real results are found and these real results are referred to as the undamped non-dimensional frequencies (λud). Since the change in imaginary values is linear, it can be expressed by the following formula.

$$\lambda_{im} = p\tau \tag{87}$$

Where p is the slope of the line. When the real value of the undamped non-dimensional frequency value becomes zero at a certain point with the increase of the viscous damping parameter, its imaginary value reaches the undamped non-dimensional frequency value. In the light of this information, at which viscous damping parameter the real value of an undamped frequency will be zero can be found approximately by the following relation.

$$\lambda_{re} = 0 \rightarrow \tau = \frac{\lambda_{ud}}{p} \tag{88}$$

The value of the viscous damping parameter calculated for the first mode can also be considered as the critical damping.

Figure 6 demonstrates the variation of the real values of the non-dimensional frequencies at C-C boundary conditions for different scale parameters (ι) due to the viscous damping parameter. It should note that the effect of damping enhances as the scale parameter (ι) grows. Figure 7 depicts the variation of imaginary values. As mentioned before, the imaginary values of the non-dimensional frequencies increase linearly as the viscous damping parameter rises. The largest slope of these lines leads the real values to zero at a viscous damping parameter smaller than the others.

Figure 8 displays the variation of the real and imaginary non-dimensional frequencies of the beam with a fixed viscous damping parameter as a function of the scale parameter. The variation of the real values is presented together with the undamped values, thus displaying the effect of the viscous damping parameter on the scale parameter. As observed in the graph, although there is an increase up to a certain point, after a certain point, it decreases faster than the increase and goes to zero. The reason for this is that, from this point onward, imaginary values exceed the real values. In this case, the viscous properties of the beam are thought to become dominant, leading to a decrease in non-dimensional frequencies. It is also noteworthy that it peaks at a constant value in all modes. On the other hand, imaginary values exhibit a similar increase to the undamped non-dimensional frequencies, reaching the undamped non-dimensional frequency values where the real values are zero. This brings us back to the point mentioned in Fig. 5.

Figure 9 demonstrates the variation of the real values of the non-dimensional frequencies at different scale parameters depending on the viscous damping parameter. It can be revealed that a plot similar to Fig. 6 appears in this case, but the effect of this scale parameter is less than that of ι. Figure 10 indicates the variation of the imaginary values and the steeper these lines are, the greater the influence of the viscous damping parameter on the real values.

Figure 11 displays the variation of the real and imaginary non-dimensional frequencies of the beam with a fixed viscous damping parameter as a function of the scale parameter. What has been mentioned for Fig. 8 can also be revealed for Fig. 11.

Figure 12 indicates the variation of the real values of the non-dimensional frequencies at different L/Ro values depending on the viscous damping parameter. When the material scale parameters are zero, the variation of L/Ro has no effect on the non-dimensional frequency. However, for positive values of the material size parameters, increasing L/Ro decreases the non-dimensional frequencies, i.e. the effect of the size parameter decreases as L/Ro grows. Thus, as illustrated in Fig. 12, the effect of damping is greater for smaller values of L/Ro. However, it should be noted that this is not due to an enhancement of L/Ro, but to a reduction in the effect of the scale parameter.

Figure 13 displays the variation of imaginary values. Figure 14 demonstrates the variation of the real and imaginary values of the non-dimensional frequencies of a nanotube with a fixed viscous damping parameter as a function of L/Ro. In order to detect the effect of damping, the variation of non-dimensional frequencies without damping is also presented in the graph with real values.

Although the effect of damping on L/Ro cannot be clearly explained by looking at this graph, it can be uncovered that the change of imaginary values is quite similar to the change of non-dimensional frequencies without damping.

Figure 15 displays the variation of the real values of the non-dimensional frequencies depending on the viscous damping parameter for three different power-law exponents. It is observed that the smaller k (power-law exponent) is, the greater the effect of damping. In addition, these effects are observed more clearly as the modes increase. Figure 16 illustrates the variation of the imaginary values of these frequencies. As mentioned before, the higher the slope of the lines indicating the change of imaginary values has greater the effect of the viscous damping parameter.

5 Conclusions

In this study, the torsional vibration of a strain gradient viscoelastic FG nanotube is realized under viscoelastic boundary conditions, which are very limited in the literature. Moreover, thanks to the viscoelastic model used, the boundary conditions can be transformed into fully elastic or fully viscous boundary conditions. When the spring constants in elastic boundary conditions have been represented by very large values, results for rigid boundary conditions, which are frequently found in the literature, can be obtained, while when they are represented by very small values, results for completely free boundary conditions can be achieved.

The results of the study have been presented below.

- The mode order of the damped non-dimensional frequencies is determined not by ordering the real values from smaller to larger, but by ordering the imaginary values from smaller to larger. Because, as the viscous damping parameter rises, the real non-dimensional frequency values in the larger modes reduce and overtake the smaller modes, even reaching zero at a certain viscous damping parameter value. It is thought that this can

be explained by the fact that the damping changes with speed and the oscillations in large modes are faster, resulting in a greater damping effect.

- The real values of the non-dimensional frequencies in the undamped state reduce curvilinearly as the viscous damping parameter grows, while the imaginary values grow linearly. However, when the real values are zero, the imaginary values reach the non-dimensional frequency value determined without damping. Hence, the relation for which mode and at which viscous damping parameter value the real value will reach zero is calculated.
- For more rigid boundary conditions the viscous damping parameter has a greater influence on the reduction of the real values of the non-dimensional frequencies. Similarly to the situation in large modes, vibration occurs more rapidly under more rigid boundary conditions. Therefore, the effect of damping may be greater in rods with more rigid boundary conditions.
- As the scale parameters build up, the effect of the viscous damping parameter on the non-dimensional frequencies rises. It is thought that the fundamental reason for this is related to the increase in stiffness amplifying the effect of damping. This increase is greatest for the ι scale parameter. This parameter reflects the strain gradient effect; therefore, it can be said that its effect on stiffness and frequency is greater. In other words effect of the γ is less compared to ι scale parameter.
- For positive values of the scale parameters, the effect of damping decreases as L/Ro grows. This can be due to the fact that the effect of the scale parameter declines as L/Ro increases. Since the dimensionless process is performed, the L/Ro change reduces the effect of these scale parameters. However, in reality, the increase in L/Ro also reduces the stiffness of the rod. In this context, the effect of damping also decreases.
- While k increases, the non-dimensional frequencies decrease due to the change in material properties. As is well known, mass and stiffness increase are the fundamental parameters affecting frequency. These parameters depend on the mechanical properties of the material forming the rod. In this context, the parameter affecting mass is density, while the parameter affecting stiffness is the elastic modulus. In a functionally graded material, the change in frequency with an increase in k is related to the extent to which these material properties change. It has also been observed that the smaller the value of k used in this study, the greater the effect of damping.

Author contributions All authors contributed equally to the manuscript.

Funding Open access funding provided by the Scientific and Technological Research Council of Türkiye (TÜBİTAK). No funding was provided for the conduct of this study.

Data availability Datasets generated during the current study are available from the corresponding author on reasonable request.

Declarations

Conflict of interest The authors have no competing interests to declare that are relevant to the content of this article.

Open Access This article is licensed under a Creative Commons Attribution 4.0 International License, which permits use, sharing, adaptation, distribution and reproduction in any medium or format, as long as you give appropriate credit to the original author(s) and the source, provide a link to the Creative Commons licence, and indicate if changes were made. The images or other third party material in this article are included in the article's Creative Commons licence, unless indicated otherwise in a credit line to the material. If material is not included in the article's Creative Commons licence and your intended use is not permitted by statutory regulation or exceeds the permitted use, you will need to obtain permission directly from the copyright holder. To view a copy of this licence, visit http://creativecommons.org/licenses/by/4.0/.

References

1. Lim CW, Zhang G, Reddy JN (2015) A higher-order nonlocal elasticity and strain gradient theory and its applications in wave propagation. J Mech Phys Solids 78:298–313. https://doi.org/10.1016/j.jmps.2015.02.001
2. Eringen AC, Author, Wegner JL, Reviewer (2003) Nonlocal continuum field theories. Appl Mech Rev 56:B20–B22. https://doi.org/10.1115/1.1553434
3. Eringen AC (1983) On differential equations of nonlocal elasticity and solutions of screw dislocation and surface waves. J Appl Phys 54:4703–4710. https://doi.org/10.1063/1.332803
4. Lam DCC, Yang F, Chong ACM, Wang J, Tong P (2003) Experiments and theory in strain gradient elasticity. J Mech Phys Solids 51:1477–1508. https://doi.org/10.1016/S0022-5096(03)00053-X
5. Yang F, Chong ACM, Lam DCC, Tong P (2002) Couple stress based strain gradient theory for elasticity. Int J Solids Struct 39:2731–2743. https://doi.org/10.1016/S0020-7683(02)00152-X
6. Aifantis EC (1999) Strain gradient interpretation of size effects. In: Bažant ZP, Rajapakse YDS (eds) Fracture scaling. Springer Netherlands, Dordrecht, pp 299–314
7. Eltaher MA, Shanab RA, Mohamed NA (2023) Analytical solution of free vibration of viscoelastic perforated nanobeam. Arch Appl Mech 93:221–243. https://doi.org/10.1007/s00419-022-02184-4
8. Yayli MÖ (2019) Free vibration analysis of a rotationally restrained (FG) nanotube. Microsyst Technol 25:3723–3734. https://doi.org/10.1007/s00542-019-04307-4
9. Trabelssi M, El-Borgi S, Fernandes R, Ke L-L (2019) Nonlocal free and forced vibration of a graded Timoshenko nanobeam resting on a nonlinear elastic foundation. Compos Part B: Eng 157:331–349. https://doi.org/10.1016/j.compositesb.2018.08.132
10. Uzun B, Yayli MÖ (2024) Rotary inertia effect on dynamic analysis of embedded FG porous nanobeams under deformable boundary conditions with the effect of neutral axis. J Braz Soc Mech Sci Eng 46:111. https://doi.org/10.1007/s40430-023-04605-z
11. Kadioglu HG, Yayli MO (2025) Dynamic analysis of rotationally restrained nanobeams made of viscoelastic functionally graded

materials. J Braz Soc Mech Sci Eng 47:262. https://doi.org/10.1007/s40430-025-05569-y
12. Balci MN (2025) Axial forced vibration problem for a viscoelastic Nanorod involving radially graded porosity. J Braz Soc Mech Sci Eng 47:203. https://doi.org/10.1007/s40430-025-05497-x
13. Ahmadi I, Najafi M, Sladek V, Sladek J (2025) Free vibration analysis of magneto-electro-elastic nanobeams in flexural and thickness modes. J Braz Soc Mech Sci Eng 48:53. https://doi.org/10.1007/s40430-025-05935-w
14. Mohammed DA, Hussein NA (2025) Effect of nonlinear damping of viscoelastic medium on torsional vibration of carbon nanotubes in a thermal environment. J Braz Soc Mech Sci Eng 47:256. https://doi.org/10.1007/s40430-025-05515-y
15. Zhen Y-X, Wen S-L, Tang Y (2019) Free vibration analysis of viscoelastic nanotubes under longitudinal magnetic field based on nonlocal strain gradient Timoshenko beam model. Physica E 105:116–124. https://doi.org/10.1016/j.physe.2018.09.005
16. Challamel N, El-Borgi S, Trabelssi M, Reddy JN (2024) Free vibration response of micromorphic Timoshenko beams. J Sound Vib 591:118602. https://doi.org/10.1016/j.jsv.2024.118602
17. El-Borgi S, Rajendran P, Trabelssi M (2023) Nonlocal and surface effects on nonlinear vibration response of a graded Timoshenko nanobeam. Arch Appl Mech 93:151–180. https://doi.org/10.1007/s00419-022-02120-6
18. Mohammadimehr M, Monajemi AA, Moradi M (2015) Vibration analysis of viscoelastic tapered micro-rod based on strain gradient theory resting on visco-pasternak foundation using DQM. J Mech Sci Technol 29:2297–2305. https://doi.org/10.1007/s12206-015-0522-2
19. El-Borgi S, Rajendran P, Friswell MI, Trabelssi M, Reddy JN (2018) Torsional vibration of size-dependent viscoelastic rods using nonlocal strain and velocity gradient theory. Compos Struct 186:274–292. https://doi.org/10.1016/j.compstruct.2017.12.002
20. Ansari R, Gholami R, Ajori S (2013) Torsional vibration analysis of carbon nanotubes based on the strain gradient theory and molecular dynamic simulations. J Vib Acoust 135. https://doi.org/10.1115/1.4024208
21. Kadioglu HG, Uzun B, Yayli MO (2025) Dynamic torsional response of viscoelastic porous nanorods with viscoelastic boundary constraints. Arab J Sci Eng. https://doi.org/10.1007/s13369-025-10208-8
22. Civalek Ö, Uzun B, Yaylı MÖ (2023) Size-dependent nonlinear stability response of perforated nano/microbeams via fourier series. Arch Appl Mech 93:4425–4443. https://doi.org/10.1007/s00419-023-02501-5
23. Akgöz B, Civalek Ö (2012) Analysis of micro-sized beams for various boundary conditions based on the strain gradient elasticity theory. Arch Appl Mech 82:423–443. https://doi.org/10.1007/s00419-011-0565-5
24. Uzun B, Civalek Ö, Yaylı MÖ (2023) Torsional and axial vibration of restrained saturated nanorods via strain gradient elasticity. Arch Appl Mech 93:1605–1630. https://doi.org/10.1007/s00419-022-02348-2
25. Uzun B, Yaylı MÖ, Civalek Ö (2024) Elastic medium and torsional spring effects on the nonlocal dynamic of functionally graded porous nanotubes. Arch Appl Mech 94:1291–1311. https://doi.org/10.1007/s00419-024-02576-8
26. Uzun B, Civalek Ö, Yaylı MÖ (2022) Axial and torsional free vibrations of restrained single-walled Boron nitride nanotube (SWBNNT) embedded in an elastic medium via nonlocal strain gradient theory. Waves Random Complex Media 1–26. https://doi.org/10.1080/17455030.2022.2147600
27. Uzun B, Yaylı MÖ, Civalek Ö (2024) An investigation on the torsional vibration of a FG strain gradient nanotube. ZAMM - Journal of applied mathematics and Mechanics /. Z für Angewandte Math Und Mechanik 104:e202301093. https://doi.org/10.1002/zamm.202301093
28. Numanoğlu HM, Civalek Ö (2019) On the torsional vibration of nanorods surrounded by elastic matrix via nonlocal FEM. Int J Mech Sci 161–162. https://doi.org/10.1016/j.ijmecsci.2019.105076
29. Khosravi F, Hosseini SA, Hamidi BA, Dimitri R, Tornabene F (2020) Nonlocal torsional vibration of elliptical nanorods with different boundary conditions. Vibration 3:189–203. https://doi.org/10.3390/vibration3030015
30. Zarezadeh E, Hosseini V, Hadi A (2020) Torsional vibration of functionally graded nano-rod under magnetic field supported by a generalized torsional foundation based on nonlocal elasticity theory. Mech Based Des Struct Mach 48:480–495. https://doi.org/10.1080/15397734.2019.1642766
31. Abdullah SS, Hosseini-Hashemi S, Hussein NA, Nazemnezhad R (2020) Temperature change effect on torsional vibration of nanorods embedded in an elastic medium using Rayleigh–Ritz method. J Braz Soc Mech Sci Eng 42:588. https://doi.org/10.1007/s40430-020-02664-0
32. Lim CW, Li C, Yu JL (2012) Free torsional vibration of nanotubes based on nonlocal stress theory. J Sound Vib 331:2798–2808. https://doi.org/10.1016/j.jsv.2012.01.016
33. Shameli R, Aghadavoudi F, Hashemian M (2023) Free torsional vibration analysis of nanorods with Non-circular Cross-Sections based on the Second-Order strain gradient theory. J Vib Eng Technol 11:3039–3055. https://doi.org/10.1007/s42417-022-00729-z
34. Selim MM, Alotaibi MF, Soltani A, Mohamed A-BA, Abdel-Aty A-H (2023) Torsional vibrational analysis of irregular single-walled carbon nanotube with elastic-support boundary conditions. J Mater Res Technol 24:215–222. https://doi.org/10.1016/j.jmrt.2023.02.230
35. Uzun B, Yayli MÖ (2024) Porosity and deformable boundary effects on the dynamic of nonlocal sigmoid and Power-Law FG nanobeams embedded in the Winkler–Pasternak medium. J Vib Eng Technol 12:3193–3212. https://doi.org/10.1007/s42417-023-01039-8
36. Uzun B, Yaylı MÖ (2024) Free vibration of a carbon Nanotube-Reinforced Nanowire/Nanobeam with movable ends. J Vib Eng Technol 12:6847–6863. https://doi.org/10.1007/s42417-024-01287-2
37. Uzun B, Kafkas U, Deliktaş B, Yaylı MÖ (2023) Size-Dependent vibration of porous bishop Nanorod with arbitrary boundary conditions and nonlocal elasticity effects. J Vib Eng Technol 11:809–826. https://doi.org/10.1007/s42417-022-00610-z
38. Kadioglu HG, Yayli MO (2025) Modified Jeffreys viscoelastic model for axial vibration of nanorods with realistic boundary conditions. Eur Phys J Plus 140:672. https://doi.org/10.1140/epjp/s13360-025-06596-3
39. Marinca B, Herisanu N, Marinca V (2023) Investigating nonlinear forced vibration of functionally graded nanobeam based on the nonlocal strain gradient theory considering mechanical impact, electromagnetic actuator, thickness effect and nonlinear foundation. Eur J Mech A Solids 102:105119. https://doi.org/10.1016/j.euromechsol.2023.105119
40. Chu L, Dui G, Zheng Y (2020) Thermally induced nonlinear dynamic analysis of temperature-dependent functionally graded flexoelectric nanobeams based on nonlocal simplified strain gradient elasticity theory. Eur J Mech A Solids 82:103999. https://doi.org/10.1016/j.euromechsol.2020.103999
41. Boyina K, Piska R, Natarajan S (2023) Nonlocal strain gradient model for thermal buckling analysis of functionally graded nanobeams. Acta Mech 234:5053–5069. https://doi.org/10.1007/s00707-023-03637-9

42. Ebrahimi F, Barati MR (2017) Hygrothermal effects on vibration characteristics of viscoelastic FG nanobeams based on nonlocal strain gradient theory. Compos Struct 159:433–444. https://doi.org/10.1016/j.compstruct.2016.09.092
43. Karamanli A (2021) Structural behaviours of zigzag and armchair nanobeams using finite element doublet mechanics. Eur J Mech A Solids 89:104287. https://doi.org/10.1016/j.euromechsol.2021.104287
44. Civalek Ö, Uzun B, Yayli MÖ (2021) Buckling analysis of nanobeams with deformable boundaries via doublet mechanics. Arch Appl Mech 91:4765–4782. https://doi.org/10.1007/s00419-021-02032-x
45. Gul U, Aydogdu M (2021) A micro/nano-scale Timoshenko-Ehrenfest beam model for bending, buckling and vibration analyses based on doublet mechanics theory. Eur J Mech A Solids 86:104199. https://doi.org/10.1016/j.euromechsol.2020.104199
46. Kadıoğlu HG, Yaylı MÖ (2025) Analysis of torsional vibration in viscoelastic functionally graded nanotubes with viscoelastic constraints using doublet mechanics theory. Int J Mech Mater Des. https://doi.org/10.1007/s10999-025-09802-3
47. Özmen R, Esen I (2023) Dynamic response of embedded Timoshenko CNTs exposed to magnetic and thermal fields subjected to moving load based on doublet mechanics. J Braz Soc Mech Sci Eng 45:590. https://doi.org/10.1007/s40430-023-04506-1
48. Ye X, Ma H, Liu X, Wei Y (2023) Size-dependent thermal bending of bilayer microbeam based on modified couple stress theory and Timoshenko beam theory. Eur J Mech A Solids 100:105029. https://doi.org/10.1016/j.euromechsol.2023.105029
49. Atcı D (2024) Nonlinear vibrations of cracked microbeams based on modified couple stress theory. Eur J Mech A Solids 106:105321. https://doi.org/10.1016/j.euromechsol.2024.105321
50. Li YS, Xiao T (2021) Free vibration of the one-dimensional piezoelectric quasicrystal microbeams based on modified couple stress theory. Appl Math Model 96:733–750. https://doi.org/10.1016/j.apm.2021.03.028
51. Tanzadeh H, Amoushahi H (2022) Buckling analysis of orthotropic nanoplates based on nonlocal strain gradient theory using the higher-order finite strip method (H-FSM). Eur J Mech A Solids 95:104622. https://doi.org/10.1016/j.euromechsol.2022.104622
52. Sun T, Guo J, Pan E (2021) Nonlocal vibration and buckling of two-dimensional layered quasicrystal nanoplates embedded in an elastic medium. Appl Math Mech -Engl Ed 42:1077–1094. https://doi.org/10.1007/s10483-021-2743-6
53. Żur KK, Arefi M, Kim J, Reddy JN (2020) Free vibration and buckling analyses of magneto-electro-elastic FGM nanoplates based on nonlocal modified higher-order sinusoidal shear deformation theory. Compos Part B: Eng 182:107601. https://doi.org/10.1016/j.compositesb.2019.107601
54. Wei L, Qing H (2022) Bending, buckling and vibration analysis of Bi-directional functionally graded Circular/Annular microplate based on MCST. Compos Struct 292:115633. https://doi.org/10.1016/j.compstruct.2022.115633
55. Le TS, Dang HT, Tran TT, Du NV, Luong HG, Pham QH (2025) Isogeometric free vibration analysis of tri-directional functionally graded nanoplates based on non-local elasticity theory. J Braz Soc Mech Sci Eng 47:263. https://doi.org/10.1007/s40430-025-05555-4
56. Qiao G, Rahmatalla S (2021) Dynamics of Euler-Bernoulli beams with unknown viscoelastic boundary conditions under a moving load. J Sound Vib 491:115771. https://doi.org/10.1016/j.jsv.2020.115771
57. Lei Y, Adhikari S, Friswell MI (2013) Vibration of nonlocal Kelvin–Voigt viscoelastic damped Timoshenko beams. Int J Eng Sci 66–67:1–13. https://doi.org/10.1016/j.ijengsci.2013.02.004
58. Lei Y, Murmu T, Adhikari S, Friswell MI (2013) Dynamic characteristics of damped viscoelastic nonlocal Euler–Bernoulli beams. Eur J Mech A Solids 42:125–136. https://doi.org/10.1016/j.euromechsol.2013.04.006
59. Hosseini-Hashemi S (2020) Vibration analysis of two-phase local/nonlocal viscoelastic nanobeams with surface effects. Eur Phys J Plus
60. Attia MA, Abdel Rahman AA (2018) On vibrations of functionally graded viscoelastic nanobeams with surface effects. Int J Eng Sci 127:1–32. https://doi.org/10.1016/j.ijengsci.2018.02.005
61. Ansari R, Faraji Oskouie M, Sadeghi F, Bazdid-Vahdati M (2015) Free vibration of fractional viscoelastic Timoshenko nanobeams using the nonlocal elasticity theory. Physica E 74:318–327. https://doi.org/10.1016/j.physe.2015.07.013
62. Mohammadimehr M, Monajemi AA, Afshari H (2020) Free and forced vibration analysis of viscoelastic damped FG-CNT reinforced micro composite beams. Microsyst Technol 26:3085–3099. https://doi.org/10.1007/s00542-017-3682-4

Publisher's Note Springer Nature remains neutral with regard to jurisdictional claims in published maps and institutional affiliations.